Anionic Contribution for Fibrous Maturation of Protofibrillar Assemblies of the Human Tau Repeat Domain in a Fluoroalcohol Solution†

Takashi Konno,*,‡ Shigetoshi Oiki,‡ Kazuhiro Hasegawa,§ and Hironobu Naiki§

Department of Molecular Physiology and Biophysics and Department of Molecular Pathology, Faculty of Medical Sciences, University of Fukui, Matsuoka, Yoshida, Fukui 910-1193, Japan

Received July 9, 2004; Revised Manuscript Received August 25, 2004

ABSTRACT: Tau protein forms fibrous aggregates in the brain of patients with Alzheimer's disease. This type of aggregation *in vitro* is promoted efficiently by polyanions and anionic micelles. Here, we report another cosolvent system that induces the fibrous aggregation of human tau four-repeat domain (τ4RD). The protein aggregation was primarily achieved by a nonanionic agent 1,1,1,3,3,3-hexafluoro-2-propanol (HFIP), while the ionic condition was modified by inorganic salts. The aggregation analysis by three spectroscopic methods revealed a two-phase kinetics of the aggregation of τ4RD in the presence of HFIP at ∼4−6%. Large increases in the light-scattering, the thioflavin-binding, and the secondary structure content of τ4RD have progressed within a few minutes at 37 °C, which was followed by another slower aggregation phase. Electron microscopic analysis demonstrated that the amorphous granules are formed in the faster step, which acquired a fibrous shape in the slower step in the solution containing NaCl. In the absence of the salt, however, the fibrous maturation was inhibited. Examination of various salt species in place of NaCl demonstrated that binding of anions to the precursor aggregates was essential for the fibrous maturation. On the basis of the results, we proposed an aggregation scheme of tau in which the formation of a thioflavin-binding intermediate occurred ahead of its fibrous maturation. The anionic environment was suggested to play a crucial role in the fibrous maturation and, therefore, could be an *in vivo* determinant of the morphology of the aggregates of tau.

Formation of neuronal intracellular inclusions of the microtubule-associated protein tau is a hallmark pathology of Alzheimer's disease (AD)[1] and other tauopathies (*1*−*4*). In the early stages of AD, the amorphous deposit of tau is formed in the brain of the patients, while the neurofibrillary tangles (NFTs) are developed in the more advanced stages of the disease (*5*, *6*). NFTs are principally composed of two types of fibrous aggregates of tau, the paired helical filament (PHF) and the straight fibers (SF) (*3*). Because the maturation of the amorphous aggregates into NFTs correlates with cognitive impairment (*6*, *7*), it is crucial to elucidate the physical mechanisms through which these changes occur.

Tau is a natively unfolded protein. Its microtubule-binding repeat domain is sufficient for forming PHF and SF and therefore contains the building principles of the fibers (*8*−*10*). However, tau and its repeat domain are highly soluble in water and hard to aggregate *in vitro* without assistance of cofactors. Up to now, two different groups of chemicals, polyanions (e.g., heparin) and anionic micelles, are known to be strong enhancers of the fibrous aggregation (*11*−*16*). Anionic sites are clustered on the surface of the cofactors, which has implicated that the anionic surface of the biological membrane or the microtubule is an *in situ* nucleation site of the fibrous aggregation of tau (*16*−*20*). The clustered anionic environment has been suggested to attract the positively charged tau repeat domains and condensate them on the surface of the macromolecular cofactors (*10*, *17*, *18*). In fact, the efficiency of the polyanions or the fatty acids for induction of the aggregation was impaired when the ionic concentration in solution was increased and the electrostatic attractive force on the anionic surface was shielded (*14*, *18*−*20*). However, it should also be noticed that the anion binding to tau would alter the protein conformation substantially, which may also be tightly coupled with the fibrously ordered assembly of tau. The enhancement of tau fibrillation by the anionic cofactors might be explained by cooperation of several different mechanisms. At present, it is also unclear whether the *in vivo* nucleation site of the fibrous aggregation of tau must be a cluster of anionic sites.

In this study, to get deeper insights into the fibrillation mechanisms of tau, we tried to induce the fibrous aggregation of the four-repeat domain of tau (τ4RD) using a solution system without polyanions or anionic micelles. A question addressed here was whether the anionic environment was

† This work was supported by a Grant-in-Aid for Scientific Research from the Ministry of Education, Science, Sports, and Culture, Japan (15659050) and CREST of the Japan Science and Technology Corporation.

* To whom correspondence should be addressed: Department of Molecular Physiology and Biophysics, Faculty of Medicine, University of Fukui, Matsuoka, Yoshida, Fukui 910-1193, Japan. Telephone: +81-776-61-8307. Fax: +81-776-61-8101. E-mail: konno@fmsrsa.fukui-med.ac.jp.

‡ Department of Molecular Physiology and Biophysics.

§ Department of Molecular Pathology.

[1] Abbreviations: AD, Alzheimer's disease; NFTs, neurofibrillary tangles; PHF, paired helical filament; SF, straight fiber; τ4RD, the four-repeat domain of human tau protein; DTT, dithiothreitol; ThT, thioflavin T; HFIP, 1,1,1,3,3,3-hexafluoro-2-propanol; TFE, 2,2,2-trifluoroethano; FTIR, Fourier transform infrared; CD, circular dichroism; TEM, transmission electron microscopy.

10.1021/bi048549o CCC: $27.50
Published on Web 10/02/2004

required for the fibrillation of τ4RD under the condition where the aggregation of τ4RD was strongly induced by nonionic cofactors. Solubility of the polypeptide backbone was reduced by alcohol (*21*), which is well-known to induce secondary structure formation, chain collapse, and assembly of polypeptide chains (*22*−*29*). Although the alcohol is often regarded as a membrane-mimicking cosolvent (*24*, *30*), its nonionic character is in clear contrast with biomembranes or other membrane-mimicking agents such as anionic detergents. Under the condition where the aggregation of τ4RD was strongly induced by the alcohol, the ionic condition was adjusted by inorganic salts such as NaCl. Using this strategy, we could find a fine solution balance that promotes the fibrous aggregation of τ4RD and cast a new light on an actual role of the anionic environment in the fibrous aggregation of tau.

MATERIALS AND METHODS

Cloning, Expression, and Purification of Recombinant τ4RD. The encoding τ4RD of cDNA was cloned by polymerase chain reaction amplification from an adult human brain cDNA library using the primers GCCAAGAGCCATATGCAGACAGCCCCCGTG and TTTGGCGTTCTCGAGGAAGGTCAGCTTGTG. The PCR-amplified fragment of τ4RD was digested with *Nde*I and *Xho*I and was ligated to the *Nde*I−*Xho*I fragment of the pET-22b vector (Novagen, EMD, Darmstadt, Germany). The correct DNA sequence was confirmed by DNA sequencing. The expression product of τ4RD contains His tags in the C-terminal portion, and the formula weight of τ4RD was 15 607. Recombinant τ4RD was purified using a standard protocol for His-tagged proteins by means of the Ni-bound chelating sepharose column (Amersham Biosciences, Chicago, IL) followed by cationic ion-exchange chromatography.

Preparation of Protein Solutions. All of the sample solutions were prepared by dissolving lyophilized τ4RD to the buffer solution containing 10 mM Tris (pH 7.5), 5 mM dithiothreitol (DTT), and 20 μM thioflavin T (ThT), with pH being adjusted by HCl. The solution additionally contained salts and 1,1,1,3,3,3-hexafluoro-2-propanol (HFIP) or 2,2,2-trifluoroethanol (TFE). ThT was purchased from Sigma−Aldrich Co. Other chemicals are of reagent grade and obtained from Nacalai Tesque Co. (Kyoto, Japan). The concentration of τ4RD was 12 μM, except for the Fourier transform infrared (FTIR) spectral measurement. The protein concentration was determined by the Bradford assay.

Kinetic Monitoring of the Aggregation of τ4RD. For monitoring kinetic changes in the light scattering and the ThT fluorescence, the sample solution in a quartz fluorescence cell (3 × 3 mm) was prepared at 10 °C in a water bath. The cell top was tightly sealed with the Parafilm. The fluorescence cell was then transferred into the sample cell folder of the fluorescence spectrometer F-2500 (Hitachi, Japan). The temperature of the cell folder was adjusted at 25 or 37 °C using a circulating water bath. The light-scattering intensity was measured with the excitation/emission wavelengths of 340 nm and the bandwidths of 2 nm. The ThT fluorescence was measured with the excitation/emission wavelengths of 440 and 480 nm and the bandwidths of 5 and 10 nm, respectively. The dead time for the temperature equilibration after the jump was about 60 s.

Circular Dichroism (CD) Spectroscopy. CD measurements of τ4RD in the far-UV region were performed using a Jasco J-820 spectropolarimeter (JASCO Co., Tokyo, Japan). A quartz cell with a path length of 0.5 mm was used. The temperature of the sample cell was controlled at 10 or 37 °C by means of the Peltier-type PTC-423S apparatus (JASCO Co.). The spectral measurements were done with the bandwidth of 1 nm, the response of 1 s, the scan rate of 100 nm/min, and the accumulation of 4 or 8 times. The kinetic change in the molar ellipticity at 220 nm ($[\theta]_{220}$) was monitored with the data interval of 5 s, the bandwidth of 5 nm, and the response of 4 s. The secondary structural analysis of the CD spectra was performed using the CDPro program package (*31*), which includes the well-established programs CONTINLL and SELCOM3, as well as two reference spectral sets. Both of the reference sets include spectra for denatured proteins. Runs of the two programs using the two data sets gave four independent estimates of the secondary structure content for each experimental spectrum of τ4RD. The average and deviation of the four values were calculated.

Transmission Electron Microscopy (TEM). TEM was performed with a H-7000 electron microscope (Hitachi, Japan) operated at 75 kV, at a magnification of 40000×. The samples were applied to carbon grids and stained with 2% uranyl acetate. The images were recorded on FG electron-microscopic films (Fuji film, Japan), developed in D-19 (Kodak) for 3 min.

FTIR Spectroscopy. FTIR spectra were measured using Jasco FT-IR 680 Plus (JASCO Co.). Atmospheric water vapor was removed by flushing the spectrometer with nitrogen. Interferograms were recorded between 1800 and 1500 cm^{-1}, and 128 spectra were averaged. They were acquired in the transition mode using a CaF2 liquid cell with a spacer of 50 μm. The reference spectra of solvents and water vapor were subtracted afterward. The samples for the FTIR measurement were prepared by dissolving 120 μM of τ4RD in D_2O containing 10 mM Tris (pD 7.5), 5 mM DTT, and 100 mM NaCl. The HFIP concentration was 0 or 4.3%. The samples were placed at 37 °C for 30 min and then transferred to the cell for the measurements.

RESULTS

Structural Change of τ4RD in the Low Concentration Range of HFIP. We tested various alcohol species including methanol, ethanol, and TFE, but only HFIP was effective in inducing the aggregation of τ4RD without assistance of ionic cofactors. The strong effect of HFIP on the conformation of τ4RD was revealed by the CD spectroscopy in the far-UV region at 25 °C. The spectrum without HFIP showed a typical pattern for a highly disordered protein conformation (Figure 1A). The spectral shape changed quite sharply at ∼4−6% HFIP (Figure 1B), developing a spectral pattern representative of a large content of secondary structures within a few minutes after the sample preparation. Turbidity of the sample solutions also increased substantially within 15 min (measured by absorbance at 340 nm). The effects of HFIP at higher concentrations than 10% were not considered in this study. The results indicated that HFIP in the relatively low concentration range was a strong inducer of the aggregation of τ4RD accompanied with the secondary structure formation. In contrast, TFE altered the CD spectrum of τ4RD more

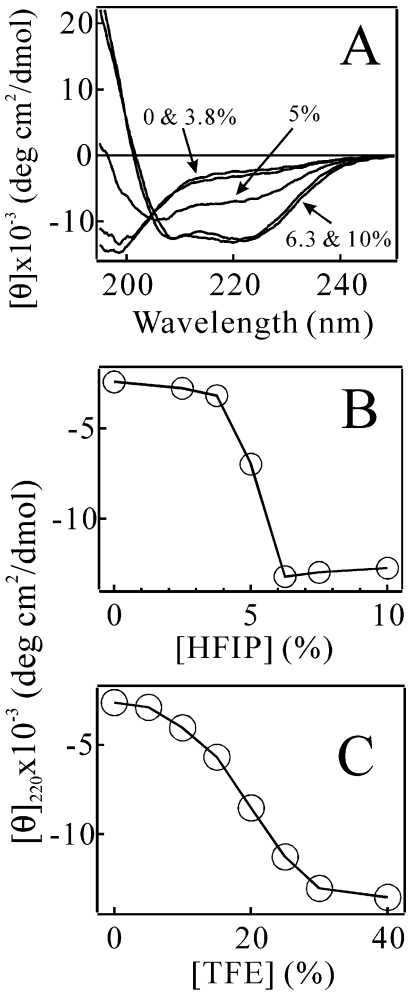

FIGURE 1: CD spectroscopic analysis of τ4RD at 25 °C. (A) CD spectra in the far-UV region at various concentrations of HFIP. The solution additionally contained 10 mM Tris (pH 7.5), 5 mM DTT, and 20 μM ThT, and the protein concentration was 12 μM. The spectra were taken within 5 min after the sample preparation. (B) Change in $[\theta]_{220}$ as a function of the concentration of HFIP. (C) Change in $[\theta]_{220}$ as a function of the concentration of TFE.

gradually (Figure 1C), and no significant increase in solution turbidity was observed.

HFIP-Induced Aggregation of τ4RD Monitored by Light Scattering and ThT Binding. The aggregation of τ4RD in the HFIP solution depended critically on the temperature, which allowed us for using a simple temperature-jump protocol. The samples were prepared at 10 °C, and the aggregation was induced by elevation of temperatures up to 37 °C (see the Materials and Methods). The aggregation kinetics was monitored by light scattering (Figure 2A), thioflavin-dye binding (Figure 2B), and $[\theta]_{220}$ (Figure 2C). Many previous reports used thioflavin S for studying the fibrous aggregation of tau (*18*), but thioflavin S slightly altered the kinetic properties of the HFIP-induced aggregation (data not shown). Instead, ThT was used because it did not have the undesirable effect. ThT is known to bind specifically to the amyloid-type aggregates of various protein species including tau (*18*, *32*, *33*). The presence of ThT did not significantly affect the results of the aggregation kinetics and the TEM experiments of this study (data not shown).

The aggregation of τ4RD could not be detected at 3.8% or the lower concentrations of HFIP at 37 °C, but a slight

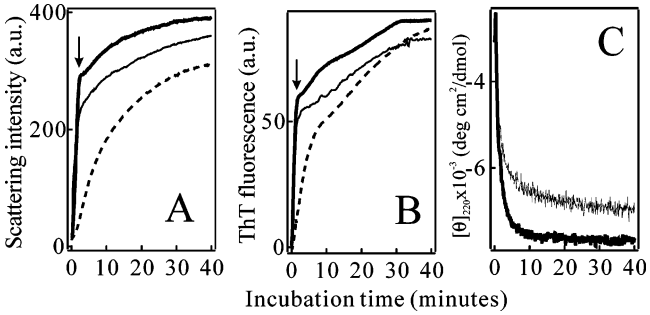

FIGURE 2: Kinetic analysis of the aggregation of τ4RD induced by HFIP monitored by the light scattering (A), ThT fluorescence (B), and $[\theta]_{220}$ (C). Thick solid lines, 100 mM NaCl and 4.3% HFIP at 37 °C; thin solid lines, 0 mM NaCl and 4.4% HFIP at 37 °C; and broken lines, 100 mM NaCl and 4.3% HFIP at 25 °C. The solutions additionally contained 10 mM Tris (pH 7.5), 5 mM DTT, and 20 μM ThT, and the protein concentration was 12 μM. Arrows in A and B indicate notches separating the faster and slower phases of the kinetic traces.

increase of HFIP up to 4.2% strongly enhanced the aggregation. The traces in Figure 2 were obtained at 4.3 or 4.4% HFIP in the presence of 0 or 100 mM NaCl. At the higher concentration of HFIP, the aggregation rate was too large to monitor by the present method. The result in Figure 2A showed that a large increase in the light-scattering intensity occurred quite rapidly within a few minutes, followed by a much slower phase. The kinetic profile obtained by the ThT-binding method was similar to that obtained by the light scattering and exhibited a two-phase pattern very clearly (Figure 2B), indicating that both of the faster and slower aggregation phases were accompanied with the enhancement of the ThT binding. Secondary structure formation of τ4RD in the aggregation process was monitored by $[\theta]_{220}$. The temperature jump from 10 to 37 °C induced the rapid reduction in $[\theta]_{220}$ (Figure 2C). It also changed in the two-phase manner (Figure 2C). Note that the amplitude of the change in the slower phase was small for the sample containing 100 mM NaCl (a thick line of Figure 2C). The results for all of the three methods demonstrated that the kinetic property of the HFIP-induced aggregation of τ4RD was not profoundly affected by the concentration of NaCl (thin lines of Figure 2). We also observed that the incubation at 25 °C substantially reduced the aggregation rates (broken lines of Figure 2). In Table 1, kinetic parameters for the faster and slower aggregation phases at 37 °C are given by fitting the traces of Figure 2 using a simple double-exponential function (see the caption of Table 1 for details).

Morphological Analysis of the Aggregates by TEM. Nanoscale morphology of the aggregates in the HFIP solution was studied by the negatively stained TEM method. In the presence of 100 mM NaCl and 4.3% HFIP, a large amount of granular aggregates was formed rapidly within 2 min of incubation at 37 °C (Figure 3A). No clear fibrous component was detected on the TEM grid. However, after a longer incubation period, the fibrous components appeared in the sample containing 100 mM NaCl (parts B and C of Figure 3). More than 80% of the aggregates on the TEM grid were fibrous in shape after the incubation for 30 min, although a precise measure of the amount ratio of the fibrous to the amorphous components could not be obtained by TEM or the other methods used in this study. These results indicated that the initial fast event of the aggregation monitored by

Table 1: Kinetic Parameters of the Aggregation Processes of τ4RD in HFIP Solutions[a]

	faster phase		slower phase	
	fraction	rate (min^{-1})	fraction	rate (min^{-1})
scattering, 0 mM NaCl[b]	0.59 ± 0.06	1.2 ± 0.5	0.41 ± 0.08	0.056 ± 0.003
scattering, 100 mM NaCl[c]	0.74 ± 0.03	0.82 ± 0.10	0.26 ± 0.03	0.056 ± 0.006
ThT, 0 mM NaCl[b]	0.53 ± 0.07	2.0 ± 1.0	0.47 ± 0.07	0.049 ± 0.010
ThT, 100 mM NaCl[c]	0.62 ± 0.03	1.5 ± 0.4	0.38 ± 0.03	0.048 ± 0.012
$[\theta]_{220}$, 0 mM NaCl[b]	0.80 ± 0.02	0.78 ± 0.11	0.20 ± 0.02	0.076 ± 0.015
$[\theta]_{220}$, 100 mM NaCl[c]	0.91 ± 0.05	0.76 ± 0.08	0.09 ± 0.05	0.080 ± 0.019

[a] Kinetic traces for the aggregation of τ4RD monitored by light scattering, ThT binding, and $[\theta]_{220}$, whose representatives are shown in Figure 2, were fitted by a double-exponential function, $A = A_0 + A_1\{f \exp(-t/\tau_1) + (1 - f) \exp(-t/\tau_2)\}$, where t is the incubation time, f and $(1 - f)$ gave the fraction parameters of the faster and slower phases, respectively, and $1/\tau_1$ and $1/\tau_2$ gave rate parameters. Each value in the table is calculated by averaging the values obtained from three independent kinetic traces. [b] 4.4% HFIP. [c] 4.3% HFIP.

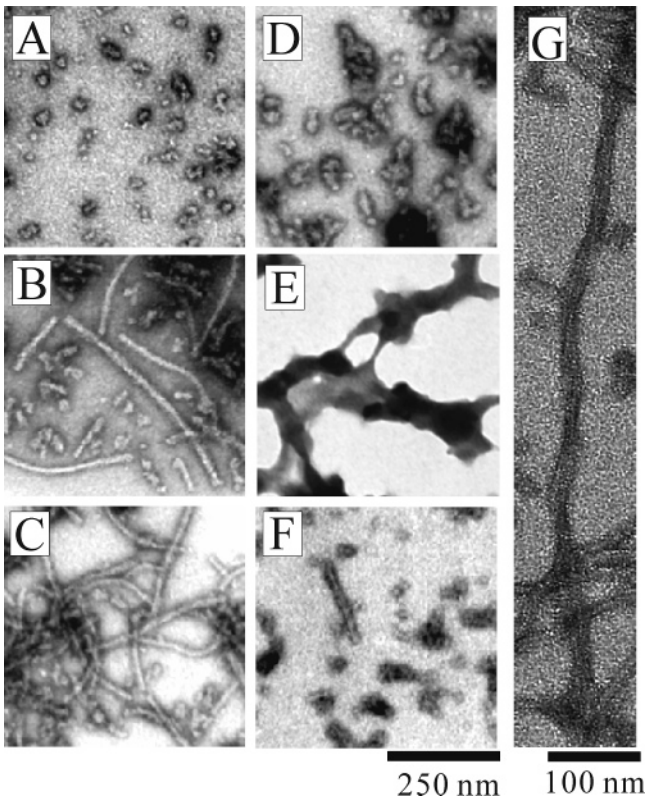

FIGURE 3: Negatively stained TEM images of τ4RD in various aggregation states. The sample containing 100 mM NaCl incubated at 37 °C for 2 min (A), 15 min (B), or 30 min (C). The sample without NaCl incubated at 37 °C for 30 min (D) and 5 h (E). The sample containing 100 mM NaCl incubated at 25 °C for 60 min (F). The sample for G is the same as that for C.

the spectroscopic methods was the formation of the granular precursor aggregates. Their maturation into the fibrous form occurred in the later phase. The PHF-type twisted fibers with crossover points were also observed in the maturated sample (Figure 3G).

In the absence of NaCl, however, the aggregates could not gain the fibrous shape in the slower step of the aggregation. After the incubation at 37 °C for 60 min, the shape of the aggregates was still amorphous (Figure 3D). Even after the incubation for several hours, the fibrous maturation was not observed, and instead, secondary segregation of the amorphous components occurred (Figure 3E). We also found that most of the aggregates formed at 25 °C were amorphous even in the presence of 100 mM NaCl, and only a few short fibers were detected (Figure 3F). When the incubation at 25 °C was prolonged for several hours, the fibrous maturation did not progress. The results of the TEM analysis demonstrated that τ4RD rapidly fell into the granular aggregation state, whereas its fibrous maturation requires the adjustments of the ionic environment and temperature.

As described above, incubation at 37 °C of τ4RD in the HFIP solution could only produce the nonfibrous granular aggregates in the absence of the salts. At various time points of this incubation, the concentration of NaCl was increased up to 150 mM, and then the samples were further incubated for 30 min. The TEM analysis was performed for these final samples. The results showed that the addition of the salt at any time points of <45 min could yield a large amount of fibrous components (data not shown). The results suggest that the granular aggregates formed in the salt-free condition are the precursor aggregates that can be maturated into fibrils with the assistance of anions.

Various salt species in place of NaCl were tested to gain insight into the mechanisms of the salt-induced fibrous maturation. The TEM analysis found that 10 mM of NaCl was not sufficient for the fibril formation of τ4RD at 4.4% HFIP (Figure 4A). Addition of 5 mM $CaCl_2$ or 3.3 mM $AlCl_3$ was similarly ineffective (parts B and C of Figure 4). In contrast, 5 mM of Na_2SO_4 or $Na_2S_2O_3$ containing divalent anions initiated fibrous aggregation to a large extent (parts D and E of Figure 4). NaSCN in 10 mM could also induce the fibrillation (Figure 4F). Note that the SCN^- anion has a stronger binding affinity to positively charged sites of proteins than the Cl^- anion (*34*). The result indicated that the anion species is a determinant for the fibrous maturation of the aggregates in the HFIP solution.

Secondary Structures of the Aggregates Formed in the HFIP Solution. For studying the secondary structure of the aggregates of τ4RD in 0 and 100 mM NaCl, the CD spectra at three different incubation times (0, 2, and 30 min) at 37 °C were measured. The existence of the isodichroic point among the three spectra at each salt concentration (arrows in Figure 5) strongly suggested that the secondary structures formed in the faster and slower aggregation phases were similar to each other. Furthermore, each spectrum in Figure 5A was quite similar in shape to the corresponding spectrum in Figure 5B, which indicated that the secondary structures of aggregates in the absence of NaCl were almost identical to those in 100 mM NaCl. To get more detailed structural information, the CD spectra were numerically analyzed using the CDPro program package (*31*). The package includes 10 reference data sets, but only 2 sets containing spectra of denatured proteins could give good fits and reasonable estimate values of the secondary structure content for the

Table 2: Secondary Structure Analysis of the CD Spectra of τ4RD and Its Aggregates in HFIP Solutions[a]

	α helix (%)	β sheet (%)	turn (%)	random (%)
0 mM NaCl, 4.4% HFIP, 10 °C	3 ± 1	15 ± 4	9 ± 3	77 ± 7
0 mM NaCl, 4.4% HFIP, 37 °C, 30 min	19 ± 2	22 ± 3	19 ± 2	40 ± 3
100 mM NaCl, 4.3% HFIP, 10 °C	1 ± 2	11 ± 5	10 ± 1	78 ± 6
100 mM NaCl, 4.3% HFIP, 37 °C, 30 min	17 ± 2	23 ± 2	18 ± 2	42 ± 7

[a] Each value is the average of four independent runs of CONTINLL and SELCOM3 using two reference data sets containing the data of denatured proteins (*31*). The spectral data used in this analysis ranged in wavelength from 194 to 240 nm (Figure 5).

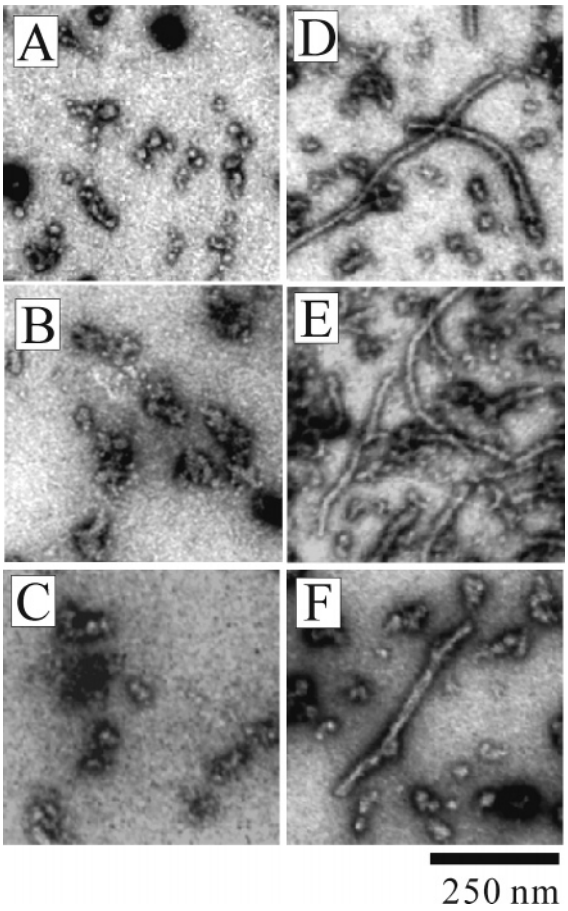

FIGURE 4: Negatively stained TEM images of the τ4RD aggregates formed by incubation for 30 min at 37 °C in the presence of 10 mM NaCl (A), 5 mM $CaCl_2$ (B), 3.3 mM $AlCl_3$ (C), 5 mM Na_2SO_4 (D), 5 mM $Na_2S_2O_3$ (E), or 10 mM NaSCN (F). The sample solutions additionally contained 10 mM Tris (pH 7.5), 5 mM DTT, 20 μM ThT, and 4.4% HFIP.

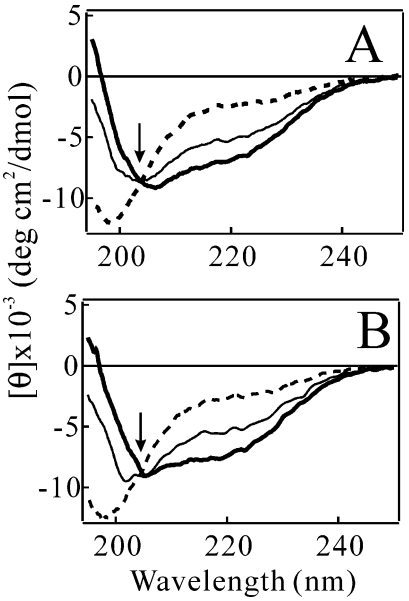

FIGURE 5: CD spectra in the far-UV region of τ4RD and its aggregates in 0 mM NaCl and 4.4% HFIP (A) or 100 mM NaCl and 4.3% HFIP (B). Broken lines, spectra at 10 °C without aggregation; thin solid lines, spectra at 37 °C for 2 min; and thick solid lines, spectra at 37 °C for 30 min. An arrow in A and B indicates an isodichroic point of three spectra.

experimental spectra of the highly disordered τ4RD (the dotted lines in Figure 5). We therefore used the 2 reference sets in the present analysis. The results in Table 2 demonstrated that all of the α-helical, β-sheet, and turn structures were formed in the aggregation process of τ4RD. It also confirmed that the secondary structures of the aggregates in the low-salt solution were almost identical to that in the solution containing 100 mM NaCl.

The amyloid-type fibrous aggregates including the core part of PHF and SF of tau are known to be rich in β-sheet structures (*35*−*39*). To confirm the β-sheet-rich conformation of τ4RD in the HFIP-induced fibrils, FTIR spectroscopy was employed. Note that the sample used for the FTIR analysis was prepared using D_2O instead of H_2O and a higher protein concentration (120 μM). The fibrous aggregation of τ4RD in this solution condition was confirmed by TEM (data not shown). The IR spectrum in the amide I region and its second derivative demonstrated that the fibrous aggregation induced by HFIP was accompanied with the appearance of the band at 1614 nm (Figure 6). This is a clear sign for the β-sheet structures and typical for the amyloid-type fibrils. At present, however, we cannot exclude the possibility that the aggregation state represented by the IR spectrum could be substantially different from that analyzed by CD because of the difference in the sample conditions.

DISCUSSION

Aggregation of τ4RD in the HFIP Solution. In this study, we searched for the solution conditions in which the fibrous aggregation of τ4RD was promoted without polyanions or anionic micelles and found that HFIP combined with simple inorganic salts enhanced the fibrillation very efficiently (Figure 3C). The amyloid-type fibers in the HFIP solution are rich in the ThT-binding sites and the β-sheet structures and also exhibited the Congo red birefringence (data not shown).

Alcohol in solution is well-known to break tertiary folds of proteins, while the unfolded protein chains take a secondary-structure-rich conformation in the alcohol solution (*22*). These alcohol effects on proteins have been argued to be membrane-mimicking (*28*, *30*, *40*), but the alcohol is the nonionic agent and therefore distinct from biomembranes or other membrane-mimicking agents such as anionic detergents. Thermodynamically, the alcohol effects have been

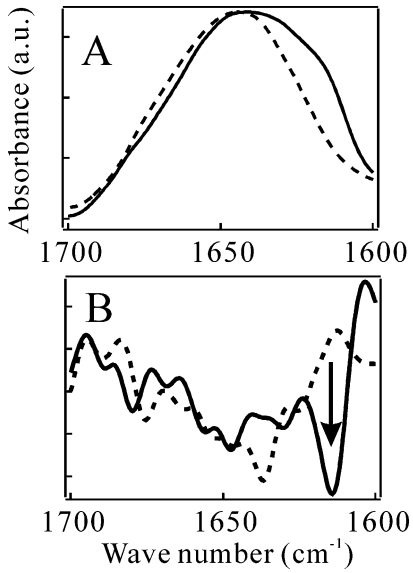

FIGURE 6: FTIR spectra (A) and their second derivatives (B) of τ4RD and its fibrous aggregates. The protein concentration was 120 μM. The sample solutions contained 10 mM Tris (pH 7.5), 5 mM DTT, and 100 mM NaCl in D_2O and were incubated at 37 °C for 30 min. Broken lines, 0% HFIP; and thin solid lines, 4.3% HFIP.

explained by a reduction in solubility of the polypeptide backbone and an increase in solubility of the hydrophobic components (*21*). Among the alcohols, HFIP and TFE are exceedingly strong agents that induce collapse and secondary structure formation of polypeptide chains (*26*, *41*). The drastic effects of the fluoroalcohols may be originated from their preferential solvation to the polypeptide components (*42*−*45*). HFIP and TFE are also known as the agents that promote amyloid-type aggregation of proteins (*28*, *46*, *47*). Consistently with these previous studies, we found that HFIP induced the aggregation of τ4RD accompanied with the formation of secondary structures (Figure 5 and Table 2) and the ThT-binding motifs (Figure 2B). The HFIP-induced aggregation of τ4RD occurred even in the low-salt solution (Figure 2), implying that no ionic cofactor was required to form the ThT-binding aggregates of the tau repeat domain. We presently observed that TFE did not induce the aggregation of τ4RD, which could be explained by the weaker effect of TFE on the polypeptide structures than that of HFIP (*26*, *41*). Addition of high concentrations of inorganic salts might induce the aggregation of τ4RD in the TFE solution, which was not tested extensively in this study.

HFIP often dissolves preformed protein aggregates or inhibits aggregation (*46*), which is in clear contrast with the present findings. It is also known that HFIP alters the morphology of the SG rod of PrP by disassembling the aggregates (*48*). We also observed that an increase in the concentration of HFIP up to 18% or more in the present experimental condition redissolved the aggregates of τ4RD preformed in the lower HFIP concentration (data not shown). It is plausible that the alcohol effect on the protein structure is varied in quality depending on the concentration range of the alcohol. In fact, we have previously observed that HFIP in a low concentration range induced collapse of an unfolded protein chain, while in the higher concentration, it induced a highly expanded helical conformation of the protein (*26*). Fink and co-workers also found that alcohols promoted aggregation of α synuclein in a variety of fashions depending on the alcohol concentrations (*28*). We would suggest that HFIP enhances the collapse or assembly of polypeptide chains in low concentrations (e.g., 5% or less), while this tendency decreases in the higher concentration range of the alcohol (e.g., >10%). It has often been argued that the secondary structure formation of unfolded protein chains in fluoroalcohol solutions well-correlated with the aggregation tendency of the proteins (*46*, *47*). However, the mechanism that underlies this phenomenon could be quite complex, where fine balancing of thermodynamic forces exerted on various polypeptide components plays a crucial role.

Fibrous Maturation of τ4RD Aggregates. The formation of the ThT-binding aggregates in the HFIP solution was, however, not sufficient for τ4RD to fall into the pathway of the fibril formation. For the fibrous maturation, the highly ionic environment was required (Figure 3). High efficiency of divalent anions and SCN^- for inducing the fibrillation (parts D−F of Figure 4), together with the relatively low effective concentration range of these anions, indicated that the direct binding of anions to the positively charged sites of τ4RD was responsible for the fibrous maturation of the precursor aggregates. However, it did not imply that the electrostatic neutralization was required for condensation of τ4RD because the intermolecular association was already enhanced very strongly by HFIP. The binding of anions to the positively charged sites of τ4RD probably modified the conformation of the precursors, which initiated their ordered arrangement into the fibers. Notably, the secondary structure composition of the fibrous aggregates was essentially the same as that of the amorphous aggregates in the low-salt solution (Figure 5 and Table 2), whereas nanoscale morphology of the aggregates was much different from each other (Figure 3). This discrepancy indicates that a minor change in the conformation of the precursor aggregates is critically important for determining their nanoscale arrangement. In contrast to the present results for HFIP, polyanions and anionic micelles induce the fibrous aggregation of tau more effectively in the lower salt solution (*14*, *18*−*20*). It is plausible that the anionic sites of these cofactors play essential roles in both attraction of tau molecules and their conformational adjustment.

The nucleation-dependent aggregation kinetics is widely common for the amyloid-type fibrous aggregation of proteins (*49*). This type of kinetics was also demonstrated for the fibrillation of tau induced by heparin (*50*) or anionic micelles (*17*, *51*). In the present condition, we observed that the kinetic rate of the precursor formation of τ4RD was much faster than the fibrous maturation step in the HFIP solution. This slow fibrillation step might be nucleation-dependent. In fact, we observed a notch separating the faster and slower steps in the kinetic traces monitored by ThT and light scattering (arrows in parts A and B of Figure 2). An improved temperature-jump protocol with a better time resolution than that used in this study is required for clarifying this point.

The scheme in Figure 7 summarizes the aggregation process of τ4RD in the HFIP solution. The granular thioflavin-binding aggregates are formed as precursors, followed by their fibrous maturation with the assistance of anions and temperature. This aggregation scheme might be valid for aggregation of tau in a variety of solution conditions and is actually consistent with the recent observation by the

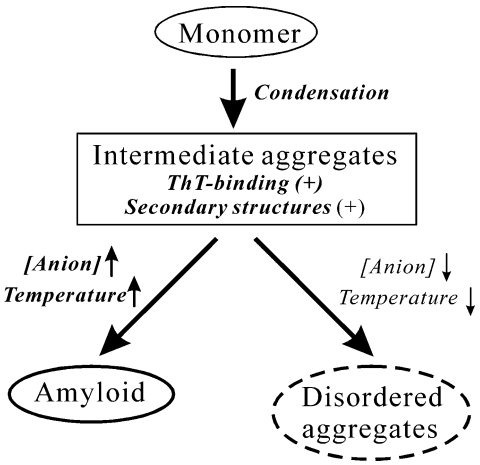

FIGURE 7: Aggregation pathway of τ4RD in the HFIP solution.

Kuret's group that the formation of a thioflavin-binding intermediate on the surface of the anionic micelles occurs ahead of the fibrous aggregation of tau (*17*). Their observation, together with our present results, suggests that the repeat domain of human tau has a strong intrinsic tendency to form the thioflavin−dye-binding motif.

Biological Implications. The negatively charged surfaces of biomembranes or microtubules are candidates for *in vivo* nucleation sites for the tau fibrillation (*16*−*20*). Previous histological studies actually observed the aggregates of tau attached to the cellular membrane components (*5*, *6*). The present study complements this view by proposing that the anionic surface is not the absolute requirement for the aggregation of tau in the cell. The biological solutions such as the intracellular fluid are very rich in organic molecules and might contain the agents that mimic the effect of HFIP. The highly crowded environment in the cell could also promote the aggregation of tau (*52*, *53*). In any case, the protein aggregation sites in the living body should be surrounded by a huge amount of molecules, some being positively charged and others being negatively charged. Hyperphosphorylation of tau observed in the brains of patients with AD (*54*) also alter the electrostatic properties of tau and its aggregates. The present study suggests that the diversity of the ionic environment could be a cause for morphological diversity of the aggregates of tau in the cell. The changes in the shape of tau aggregate in the patients with AD from an amorphous to a fibrous one (*5*, *6*) might be originated from the ionic mechanisms.

Concluding Remarks. The study on the fibrillation mechanism of tau has been greatly advanced by the previous finding that polyanions and anionic micelles enhanced the tau aggregation *in vitro* (*9*, *10*, *55*). The present study found another cosolvent system that induces the fibrous aggregation of the core part of tau. The flexibility of the present system allowed us to inspect the actual role of anions in forming the fibrous aggregates. Further studies on the structure of the HFIP-induced fiber are required to elucidate its relation to PHF and SF of the patients with AD. Furthermore, the experimental probe that precisely measures the amount ratio of the fibrous to amorphous components of tau aggregates must be developed for a more advanced study of the molecular mechanism that determines the morphology of the tau aggregates.

ACKNOWLEDGMENT

We thank Mr. Hitoshi Takagi (Center for Biomedical Research, University of Fukui) for his technical assistance in the TEM experiments.

REFERENCES

1. Buee, L., Bussiere, T., Buee-Scherrer, V., Delacourte, A., and Hof, P. R. (2000) Tau protein isoforms, phosphorylation, and role in neurodegenerative disorders, *Brain. Res. Rev. 33*, 95−130.
2. Garcia, M. L., and Cleveland, D. W. (2001) Going new places using an old MAP: Tau, microtubules, and human neurodegenerative disease, *Curr. Opin. Cell Biol. 13*, 41−48.
3. Goedert, M., Spillantini, M. G., and Davies, S. W. (1998) Filamentous nerve cell inclusions in neurodegenerative diseases, *Curr. Opin. Neurobiol. 8*, 619−632.
4. Avila, J., Lucas, J. J., Perez, M., and Hernandez, F. (2004) Role of tau protein in both physiological and pathological conditions, *Physiol. Rev. 84*, 361−384.
5. Mena, R., Edwards, P. C., Harrington, C. R., Mukaetova-Ladinska, E. B., and Wischik, C. M. (1996) Staging the pathological assembly of truncated tau protein into paired helical filaments in Alzheimer's disease, *Acta Neuropathol. 91*, 633−641.
6. Galvan, M., David, J. P., Delacourte, A., Luna, J., and Mena, R. (2001) Sequence of neurofibrillary changes in aging and Alzheimer's disease: A confocal study with phospho-tau antibody, AD2, *J. Alzheimer's Dis. 3*, 417−425.
7. Garcia-Sierra, F., Hauw, J. J., Duyckaerts, C., Wischik, C. M., Luna-Munoz, J., and Mena, R. (2000) The extent of neurofibrillary pathology in perforant pathway neurons is the key determinant of dementia in the very old, *Acta Neuropathol. 100*, 29−35.
8. Mandelkow, E. M., and Mandelkow, E. (1998) Tau in Alzheimer's disease, *Trends Cell Biol. 8*, 425−427.
9. Friedhoff, P., von Bergen, M., Mandelkow, E. M., and Mandelkow, E. (2000) Structure of tau protein and assembly into paired helical filaments, *Biochim. Biophys. Acta 1502*, 122−132.
10. Gamblin, T. C., Berry, R. W., and Binder, L. I. (2003) Modeling tau polymerization *in vitro*: A review and synthesis, *Biochemistry 42*, 15009−15017.
11. Goedert, M., Jakes, R., Spillantini, M. G., Hasegawa, M., Smith, M. J., and Crowther, R. A. (1996) Assembly of microtubule-associated protein tau into Alzheimer-like filaments induced by sulphated glycosaminoglycans, *Nature 383*, 550−553.
12. Perez, M., Valpuesta, J. M., Medina, M., Montejo de Garcini, E., and Avila, J. (1996) Polymerization of tau into filaments in the presence of heparin: The minimal sequence required for tau−tau interaction, *J. Neurochem. 67*, 1183−1190.
13. Kampers, T., Friedhoff, P., Biernat, J., Mandelkow, E. M., and Mandelkow, E. (1996) RNA stimulates aggregation of microtubule-associated protein tau into Alzheimer-like paired helical filaments, *FEBS Lett. 399*, 344−349.
14. Wilson, D. M., and Binder, L. I. (1997) Free fatty acids stimulate the polymerization of tau and amyloid β peptides. *In vitro* evidence for a common effector of pathogenesis in Alzheimer's disease, *Am. J. Pathol. 150*, 2181−2195.
15. King, M. E., Gamblin, T. C., Kuret, J., and Binder, L. I. (2000) Differential assembly of human tau isoforms in the presence of arachidonic acid, *J. Neurochem. 74*, 1749−1757.
16. Chirita, C. N., Necula, M., and Kuret, J. (2003) Anionic micelles and vesicles induce tau fibrillization *in vitro*, *J. Biol. Chem. 278*, 25644−25650.
17. Chirita, C. N., and Kuret, J. (2004) Evidence for an intermediate in tau filament formation, *Biochemistry 43*, 1704−1714.
18. Friedhoff, P., Schneider, A., Mandelkow, E. M., and Mandelkow, E. (1998) Rapid assembly of Alzheimer-like paired helical filaments from microtubule-associated protein tau monitored by fluorescence in solution, *Biochemistry 37*, 10223−10230.
19. Ackmann, M., Wiech, H., and Mandelkow, E. (2000) Nonsaturable binding indicates clustering of tau on the microtubule surface in a paired helical filament-like conformation, *J. Biol. Chem. 275*, 30335−30343.
20. Makrides, V., Shen, T. E., Bhatia, R., Smith, B. L., Thimm, J., Lal, R., and Feinstein, S. C. (2003) Microtubule-dependent oligomerization of tau. Implications for physiological tau function and tauopathies, *J. Biol. Chem. 278*, 33298−33304.

21. Nozaki, Y., and Tanford, C. (1971) The solubility of amino acids and two glycine peptides in aqueous ethanol and dioxane solutions. Establishment of a hydrophobicity scale, *J. Biol. Chem. 246*, 2211−2217.
22. Buck, M. (1998) Trifluoroethanol and colleagues: Cosolvents come of age. Recent studies with peptides and proteins, *Q. Rev. Biophys. 31*, 297−355.
23. Chiti, F., Taddei, N., Webster, P., Hamada, D., Fiaschi, T., Ramponi, G. and Dobson, C. M. (1999) Acceleration of the folding of acylphosphatase by stabilization of local secondary structure, *Nat. Struct. Biol. 6*, 380−387.
24. Kamatari, Y. O., Ohji, S., Konno, T., Seki, Y., Soda, K., Kataoka, M., and Akasaka, K. (1999) The compact and expanded denatured conformations of apomyoglobin in the methanol−water solvent, *Protein Sci. 8*, 873−882.
25. Ohnishi, S., Koide, A., and Koide, S. (2000) Solution conformation and amyloid-like fibril formation of a polar peptide derived from a β-hairpin in the OspA single-layer β-sheet, *J. Mol. Biol. 301*, 477−489.
26. Konno, T., Iwashita, J., and Nagayama, K. (2000) Fluorinated alcohol, the third group of cosolvents that stabilize the molten-globule state relative to a highly denatured state of cytochrome *c*, *Protein Sci. 9*, 564−569.
27. Chiti, F., Taddei, N., Bucciantini, M., White, P., Ramponi, G., and Dobson, C. M. (2000) Mutational analysis of the propensity for amyloid formation by a globular protein, *EMBO J. 19*, 1441−1449.
28. Munishkina, L. A., Phelan, C., Uversky, V. N., and Fink, A. L. (2003) Conformational behavior and aggregation of α-synuclein in organic solvents: Modeling the effects of membranes, *Biochemistry 42*, 2720−2730.
29. Yamamoto, S., Yamaguchi, I., Hasegawa, K., Tsutsumi, S., Goto, Y., Gejyo, F., and Naiki, H. (2004) Glycosaminoglycans enhance the trifluoroethanol-induced extension of β 2-microglobulin-related amyloid fibrils at a neutral pH, *J. Am. Soc. Nephrol. 15*, 126−133.
30. Bychkova, V. E., Dujsekina, A. E., Klenin, S. I., Tiktopulo, E. I., Uversky, V. N., and Ptitsyn, O. B. (1996) Molten globule-like state of cytochrome *c* under conditions simulating those near the membrane surface, *Biochemistry 35*, 6058−6063.
31. Sreerama, N., Venyaminov, S. Y., and Woody, R. W. (2000) Estimation of protein secondary structure from circular dichroism spectra: Inclusion of denatured proteins with native proteins in the analysis, *Anal. Biochem. 287*, 243−251.
32. Wisniewski, H. M., Wen, G. Y., and Kim, K. S. (1989) Comparison of four staining methods on the detection of neuritic plaques, *Acta Neuropathol. 78*, 22−27.
33. Roher, A. E., Palmer, K. C., Chau, V., and Ball, M. J. (1988) Isolation and chemical characterization of Alzheimer's disease paired helical filament cytoskeletons: Differentiation from amyloid plaque core protein, *J. Cell Biol. 107*, 2703−2716.
34. Gjerde, D. T., Schmuckler, G., and Fritz, J. S. (1980) Anion chromatography with low-conductivity eluents. II, *J. Chromatogr. 187*, 35−45.
35. Sunde, M., and Blake, C. C. (1998) From the globular to the fibrous state: Protein structure and structural conversion in amyloid formation, *Q. Rev. Biophys. 31*, 1−39.
36. von Bergen, M., Friedhoff, P., Biernat, J., Heberle, J., Mandelkow, E. M., and Mandelkow, E. (2000) Assembly of tau protein into Alzheimer paired helical filaments depends on a local sequence motif ((306)VQIVYK(311)) forming β structure, *Proc. Natl. Acad. Sci. U.S.A. 97*, 5129−5134.
37. Abraha, A., Ghoshal, N., Gamblin, T. C., Cryns, V., Berry, R. W., Kuret, J., and Binder, L. I. (2000) C-terminal inhibition of tau assembly *in vitro* and in Alzheimer's disease, *J. Cell Sci. 113* (Part 21), 3737−3745.
38. Giannetti, A. M., Lindwall, G., Chau, M. F., Radeke, M. J., Feinstein, S. C., and Kohlstaedt, L. A. (2000) Fibers of tau fragments, but not full length tau, exhibit a cross β-structure: Implications for the formation of paired helical filaments, *Protein Sci. 9*, 2427−2435.
39. Barghorn, S., Davies, P., and Mandelkow, E. (2004) Tau paired helical filaments from Alzheimer's disease brain and assembled *in vitro* are based on β-structure in the core domain, *Biochemistry 43*, 1694−1703.
40. Kamatari, Y. O., Konno, T., Kataoka, M., and Akasaka, K. (1996) The methanol-induced globular and expanded denatured states of cytochrome *c*: A study by CD fluorescence, NMR, and small-angle X-ray scattering, *J. Mol. Biol. 259*, 512−523.
41. Hirota, N., Mizuno, K., and Goto, Y. (1998) Group additive contributions to the alcohol-induced α-helix formation of melittin: Implication for the mechanism of the alcohol effects on proteins, *J. Mol. Biol. 275*, 365−378.
42. Diaz, M. D., Fioroni, M., Burger, K., and Berger, S. (2002) Evidence of complete hydrophobic coating of bombesin by trifluoroethanol in aqueous solution: An NMR spectroscopic and molecular dynamics study, *Chemistry 8*, 1663−1669.
43. Fioroni, M., Diaz, M. D., Burger, K., and Berger, S. (2002) Solvation phenomena of a tetrapeptide in water/trifluoroethanol and water/ethanol mixtures: A diffusion NMR, intermolecular NOE, and molecular dynamics study, *J. Am. Chem. Soc. 124*, 7737−7744.
44. Gast, K., Siemer, A., Zirwer, D., and Damaschun, G. (2001) Fluoroalcohol-induced structural changes of proteins: Some aspects of cosolvent−protein interactions, *Eur. Biophys. J. 30*, 273−283.
45. Roccatano, D., Colombo, G., Fioroni, M., and Mark, A. E. (2002) Mechanism by which 2,2,2-trifluoroethanol/water mixtures stabilize secondary-structure formation in peptides: A molecular dynamics study, *Proc. Natl. Acad. Sci. U.S.A. 99*, 12179−12184.
46. Padrick, S. B. and Miranker, A. D. (2002) Islet amyloid: Phase partitioning and secondary nucleation are central to the mechanism of fibrillogenesis, *Biochemistry 41*, 4694−4703.
47. Fezoui, Y., and Teplow, D. B. (2002) Kinetic studies of amyloid β-protein fibril assembly, *J. Biol. Chem. 277*, 36948−36954.
48. Wille, H., Zhang, G.-F., Baldwin, M. A., Cohen, F. E. and Prusiner, S. B. (1996) Separation of scrapie prion infectivity from PrP amyloid polymers, *J. Mol. Biol. 259*, 608−621.
49. Harper, J. D., and Lansbury, P. T., Jr. (1997) Models of amyloid seeding in Alzheimer's disease and scrapie: Mechanistic truths and physiological consequences of the time-dependent solubility of amyloid proteins, *Annu. Rev. Biochem. 66*, 385−407.
50. Friedhoff, P., von Bergen, M., Mandelkow, E. M., Davies, P., and Mandelkow, E. (1998) A nucleated assembly mechanism of Alzheimer paired helical filaments, *Proc. Natl. Acad. Sci. U.S.A. 95*, 15712−15727.
51. King, M. E., Ahuja, V., Binder, L. I., and Kuret, J. (1999) Ligand-dependent tau filament formation: Implications for Alzheimer's disease progression, *Biochemistry 38*, 14851−14859.
52. Minton, A. P. (2001) The influence of macromolecular crowding and macromolecular confinement on biochemical reactions in physiological media, *J. Biol. Chem. 276*, 10577−10580.
53. Ellis, R. J. (2001) Macromolecular crowding: Obvious but underappreciated, *Trends Biochem. Sci. 26*, 597−604.
54. Bancher, C., Brunner, C., Lassmann, H., Budka, H., Jellinger, K., Wiche, G., Seitelberger, F., Grundke-Iqbal, I., Iqbal, K., and Wisniewski, H. M. (1989) Accumulation of abnormally phosphorylated tau precedes the formation of neurofibrillary tangles in Alzheimer's disease, *Brain Res. 477*, 90−99.
55. Barghorn, S., and Mandelkow, E. (2002) Toward a unified scheme for the aggregation of tau into Alzheimer paired helical filaments, *Biochemistry 41*, 14885−14896.

BI048549O